Heliyon 10 (2024) e31499

Contents lists available at ScienceDirect

Heliyon

journal homepage: www.cell.com/heliyon

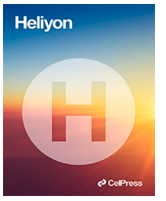

Research article

Chemical radioanalysis of production of positron-emitting radioisotope Gallium-68 via (p,n) and (p,2n) reactions using compact cyclotron for tomography applications

Abdollah Khorshidi [a,b]

[a] School of Paramedical, Gerash University of Medical Sciences, Gerash, Iran
[b] Soleimani Maktab, Central Branch, Qaem University, Kerman, Iran

ARTICLE INFO

Keywords:
^{68}Zn(p,n) and ^{69}Ga(p,2n) reactions
Compact cyclotron
Positron emitter ^{68}Ga
Saturation activity
Production yield
Neural network

ABSTRACT

In this study, the proton-induced reactions of ^{68}Zn and ^{69}Ga aimed at generating ^{68}Ga were simulated and modeled using Talys code and neural network software. In the first step, both targets were simulated under different proton energies and at different bombardments times to generate a total of six thousand data. Then, the obtained data from the Talys, including the various cross-sections, contaminations, the main product i.e. ^{68}Ga, and other options were completely saved in the output file. Afterwards, the inputs of the neural network were selected from the output of the Talys by analyzing and considering most of the key features. A total of four inputs, two of which are different energies related to the reaction, the other is the process sequence and the fourth input is the bombardment time, were recognized as suitable inputs and the model was trained differently depending on the type of target. The selected model was a feed-forward neural network with 5 nodes in a middle layer, which was able to estimate the output of Talys code by changing the input parameters with extremely high accuracy. Two different models including the main model for estimating the output of the main sample (product) and the sub-model for estimating process pollution or impurity were trained, and then the trained model was tested on the deduced process data. The implementation results fully demonstrated the high accuracy of the method. The neural network model is much easier to implement than the Talys code, and its execution speed is very high. In addition, it can be used appropriately as a system alternative for optimization and different structures in medical and biological engineering.

1. Introduction

Nowadays, the applications of nuclear technology have become very diverse and have gained special place in various fields such as nuclear medicine, agriculture, industry and radionuclide production [1–8]. The application of nuclear medicine for treatment and diagnosis using radioisotopes was first made in 1937, and radioisotopes were used as tracers in imaging in 1924 [9]. The evaluation of nuclear data has a long history, a rationalized data format and supercomputing-capable calculations will merely further progress a library that has already come a long way since its inception in 1968 [10]. The first nuclear data library dates back to the 1950s [11]. At that time, the quantitative analysis of nuclear reactions was just the projectile of a few scattered points of experimental data, and there was no method to access the full form of information. However, the basic reactor physics codes available at that time made it possible

E-mail addresses: abkhorshidi@yahoo.com, abkhorshidi@chmail.ir.

https://doi.org/10.1016/j.heliyon.2024.e31499
Received 18 January 2024; Received in revised form 16 May 2024; Accepted 16 May 2024
Available online 17 May 2024

to predict the characteristics of reactors and other critical systems. In nuclear modeling, relatively simple optical models, surface densities, composite nuclear models are used to estimate the measured cross-sections [12–14]. During the 1980s and 1990s, various nuclear model codes became available. The idea of creating a Talys code was proposed in 1998 and was available in the market for a decade or more [15]. Entering these codes is proportional in the details of the input parameters.

Gallium-68 (^{68}Ga) is produced from the decay of germanium-68 (^{68}Ge) with a relatively high half-life of 270 days, known as ^{68}Ge/^{68}Ga generator. Today, gallium is known as one of the suitable radioisotopes in nuclear medicine for PET imaging. This radioisotope decays to the stable radioisotope zinc-68 (^{68}Zn) with a half-life of 68 min and emits a positron with a maximum energy of 1.97 MeV (89 %), electron capture (11 %), and finally gamma rays with an energy of 1.077 MeV [16]. The average positron energy of ^{68}Ga is 0.83 MeV, resulting in an average positron range of 0.35 cm. The practical half-life of ^{68}Ga by $T_{1/2} = 68$ min provides satisfactory radioactivity for different PET applications while delivering adequate radiation doses to the patients. Fig. 1 shows the decay scheme of ^{68}Ge/^{68}Ga to reach a stable radioisotope of ^{68}Zn via electron capture and positron decay procedures.

The cation of $^{68}Ga^{3+}$ be able to cause stable complexes with different ligands that comprise nitrogen and oxygen as donor atoms. At this situations, ^{68}Ga is suitable for complexation with numerous macromolecules and chelators, which enables the development of kits [17]. The content of the emitted particles and the energy range affect the obtained resolution in imaging. ^{68}Ga has greater positron kinetic energy, and therefore higher positron range, and is anticipated to possess a lower spatial image resolution compared to ^{18}F with average positron energy of 0.25 MeV and maximum of 0.63 MeV. Nevertheless, both experimental measurements and computational analyzes indicates a similarly great image quality for these two radionuclides with an assumed detector or scanner resolution of 2.5–4 mm [18,19]. Meanwhile, ^{68}Ga equals the biological half-life of various peptides utilized for positron imaging by virtue of its localization to the target, rapid blood clearance, and rapid diffusion. In the clinical use of ^{68}Ga compared to ^{18}F, the time between injection and scan to transfer activity from blood to tissue is an important factor that highlights the role of half-life. The half-life of ^{68}Ga and ^{18}F is 1.13 and 1.83 h, respectively. Since ^{68}Ga (89.14 %) has a lower positron efficiency than ^{18}F (96.86 %), as a result, its detection sensitivity will also be lower [20]. Radiochemically, the half-life of ^{68}Ga ($T_{1/2} = 68$ min) provides sufficient radioactivity for various PET imaging applications to deliver acceptable doses of radiation to patients through the development of different kits with distinct macromolecules and chelators.

In this research through a medium-range of cyclotron located in Karaj city of Iran, ^{68}Zn(p,n)^{68}Ga as direct reaction and ^{69}Ga (p,2n)^{68}Ge→^{68}Ga as indirect reaction of generator are simulated by Talys code. Then, the Talys outputs are implemented in a neural network model to estimate the main output of the process besides the pollution outputs and the process loss based on the input parameters changes.

2. Methods and materials

2.1. Talys code simulation

The Talys code has been prepared and developed by Dr. Arjan Koning and his colleagues in the Netherlands [15]. This calculation code has been intended for nuclear reactions in which the particles thrown towards the target can be neutrons, protons, deuterons, etc. This code can be run on Linux and Unix operating systems. In the Talys code, a series of inputs are required, including:

A) Target mass number.
B) Input energy of the projectile to hit the target.
C) The name of the projectile.
D) The name of the target element.

Using a computer code is a proper way to simulate nuclear reactions, since nuclear experiments with limited facilities are expensive. This code can be used to find kernel models that better describe the interaction. Also, this code performs better and is easier to implement than Alice code. Talys is a software for analyzing and predicting nuclear reactions that is widely used for basic and applied sciences.

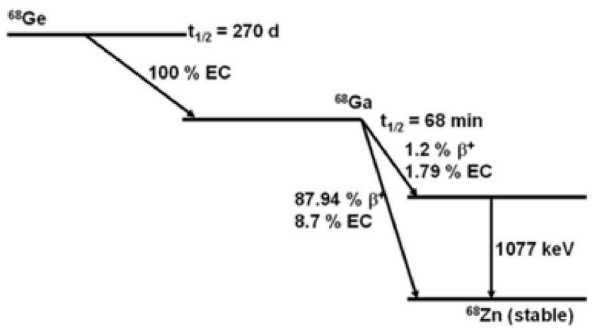

Fig. 1. Decay scheme of ^{68}Ge/^{68}Ga generator towards stable radioisotope of ^{68}Zn. [EC is electron capture and β^+ is positron decay].

Important applications that directly or indirectly depend on the data generated by the nuclear reaction simulation codes are as follows: Conventional and modern nuclear power reactors, transport of radioactive waste, fusion reactors, applications of accelerators, national security, production of medicinal isotopes, radiotherapy, drilling an oil well, geophysics and astronomical physics. In this research, the process of input and output data for proton irradiation on ^{68}Zn target by Talys code is investigated as follows,

#General.
Projectile p.
Element Zn.
Mass 68.
Energy 10 14 0.5 # E_{beam} from 10 MeV to 14 MeV with 0.5 MeV intervals.
Also, ^{69}Ga target was simulated under proton beam irradiation as:
#General.
Projectile p.
Element Ga.
Mass 69.
Energy 15 30 0.5 # E_{beam} from 15 MeV to 30 MeV with 0.5 MeV intervals.

Since the derivation of two neutrons by an incident proton requires more energy, a proton beam with an energy of 15–30 MeV was considered for the ^{69}Ga(p,2n)^{68}Ge reaction. Fig. 2 compares the cross sections of (p, n/2n/3n) reactions in terms of incident proton energy for ^{68}Zn and ^{69}Ga targets.

When the target is irradiated to reach the main product, competitive reactions always occur, which affect the quality of the main product and also reduce the production quantity. Therefore, to control and monitor competing or parallel reactions, appropriate targets such as natural gallium and ^{65}Cu are used alongside the main target, which is irradiated simultaneously with the main target in experiment.

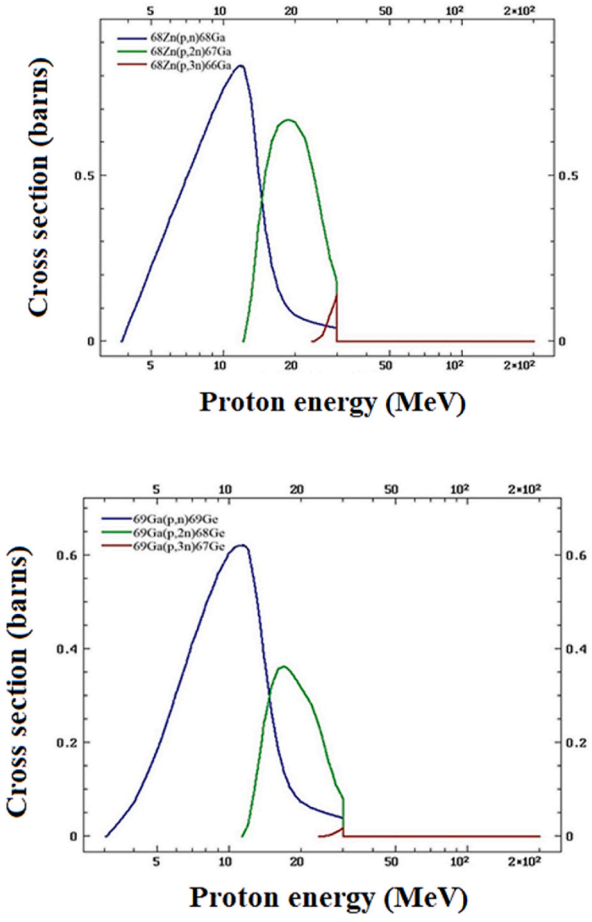

Fig. 2. Comparison of (p,n), (p,2n), and (p,3n) reactions for the targets ^{68}Zn (Top) and ^{69}Ga (Bottom).

2.2. Neural network modelling

An artificial neural network is actually a simple model of a biological neural network and it is a kind of learning and trainable system. In fact, the neural network works is such that it models the relationship between input and output without any specific or complex mathematical model. The artificial neural network is based on the following properties as a generalization of the mathematical model of human or bio-neural recognition:

A) Information processing occurs in a series of simple elements called nerve cells.
B) The signal is exchanged between nerve cells through the connections between them.
C) Each connection is assigned a weight, which is multiplied by the transmitted signal in the artificial neural network. Fig. 3 shows the block diagram of neural network modelling.

Neural network applications include: Calculation of a known function, approximation of an unknown function, pattern recognition, signal processing, and learning or training to do the aforementioned items.

A multilayer feed-forward neural network is projected as shown in Fig. 4. The Levenberg-Marquardt-Back-Propagation method is regularly selected for training artificial neural network (ANN) design in order to raise the convergence speed and prevent long teaching or training times. This algorithm is established upon numerical optimization procedures and is a universal form of the LMS (Least Mean Square) algorithm [21,22]. Meanwhile, back-propagation method is an estimated severest fall-off algorithm where the performance index is the MSE (Mean Square Error). The difference between back-propagation and LMS algorithm lies in the way the derivatives are computed. Obviously, the relationship between network weights and error for a multilayer network with nonlinear transfer functions is more complex than in a single layer network [23]. At this situation, the chain law is normally utilized to compute the derivatives. The back-propagation technique is typically utilized in controlled learning and the input data besides preferred outputs are afforded to the network. Subsequently, the network weight matrix is restructured and attuned to diminish the error function by computing the gradient of the error function.

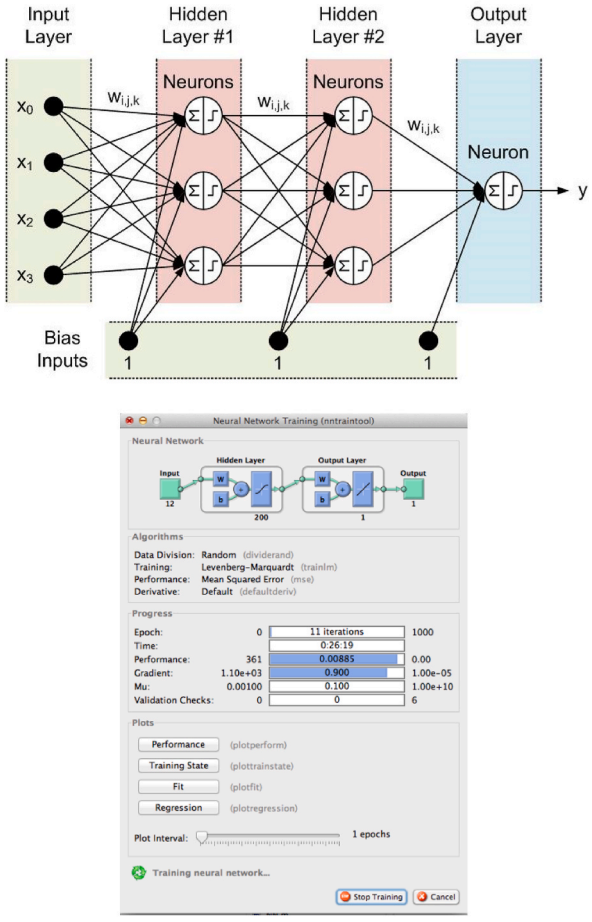

Fig. 3. Neural network modelling process via nerve cells connections (Top); Neural network in training neural nets in MATLAB toolbox including Epoch, Time, Performance, Gradient, Mu, and Validation checks (Bottom).

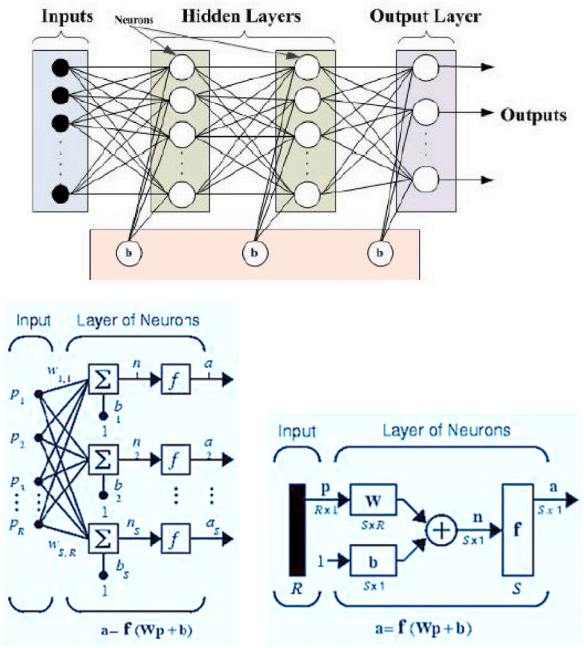

Fig. 4. The scheme of feed-forward neural network (Top) besides its mathematical explanations (Bottom) where *p*, *w*, *f*, *b*, *R* and *S* are input data, weight matrix, transfer or activation function, bias vector, number of elements in input vector, and number of neurons in layer, respectively. Meanwhile, *n* and *a* parameters indicate input and output of log-sigmoid transfer function as $a = logsig(n)$ [For more details, see supplementary file].

The obtained data from the Talys, including the various cross-sections, contaminations, the main product i.e. ^{68}Ga, and other particle history options were completely saved in the output file. Then, the output from Talys was implemented as input to the neural network of MATLAB software. The designed program was adopted so that it can read all the outputs of Talys automatically and based on the parameters changed in the input, it considers the useful outputs and the equivalent outlier outputs separately, and then, adds the outlier outputs together and generates a data for neural network training. To properly train the network, a total of six thousand different modes of Talys code were run and the results saved to separate output files. The program designed by MATLAB software automatically reads the set of six thousand files and extracts the desired data for training the neural network. Finally, a feed-forward neural network with the number of middle layer nodes 5 and one middle layer to provide the appropriate output was the best recognized state. The network training algorithm was based on the "back-propagation-error" pattern, which is comparatively investigated here.

Two feed-forward neural networks with "back-propagation-error" pattern were trained in a form that can model the main output of the process and the equivalent outputs of pollution or process outliers based on the input parameters and their changes.

3. Results

Fig. 5 compares the various cross-sections for direct reaction of ^{68}Zn(p,n)^{68}Ga [24–37] with an overall uncertainty of 7.4 % in terms

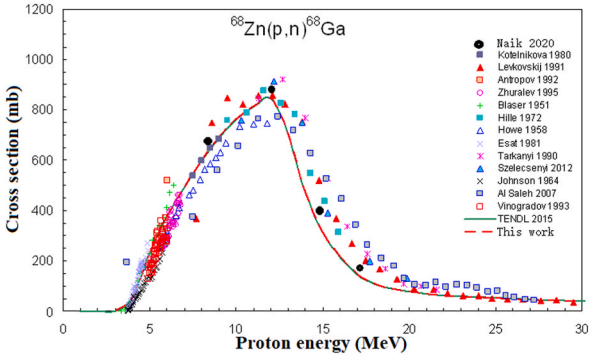

Fig. 5. The cross sections in terms of incident proton energy for the ^{68}Zn(p,n)^{68}Ga reaction [24–37].

of incident proton energy. It indicates that the maximum probability of the reaction occurs between 10 and 14 MeV of proton energy for (p,n) reaction. At this energy range, the maximum cross-section was about 0.9 b. Also, Fig. 6 shows the obtained production yield with threshold energy of 4 MeV so that with the increase of incident proton energy, the yield value also increases. The computed yields for ^{68}Zn(p,n)^{68}Ga reaction were 2820 and 7600 MBq/μA.h for 10 and 14 MeV proton energy, respectively. Meanwhile, the saturation activities for 1 μA irradiation were 4600 and 12400 MBq/μA, correspondingly.

Fig. 7 compares different cross-sections for indirect reaction of ^{69}Ga(p,2n)^{68}Ge [26,38–40] along with an overall uncertainty of 12.1 % in terms of incident proton energy. It demonstrates that the maximum probability of the reaction occurs between 15 and 30 MeV of proton energy for (p,2n) reaction. The maximum cross-section was about 0.5 b. Meanwhile, Fig. 8 displays the acquired production yield with threshold energy of 12 MeV as the incident proton energy increases, the yield value also raises. The computed yields for ^{69}Ga(p,2n)^{68}Ge reaction were 0.116, 0.807, 1.71, and 2.29 MBq/μA.h for 15, 20, 25, and 30 MeV proton energy, respectively. Meanwhile, the saturation activities for 1 μA irradiation were 1090, 7570, 16000, and 21500 MBq/μA, correspondingly.

Fig. 9 shows very good agreement between the output of Talys and the output of the model designed by the neural network in the main output of Zn-68 process. The “plus” data signs are the output of the trained neural network model and the “circle” data signs are the output of the Talys code. In order to show the effectiveness of the training, Fig. 10 shows the mean square error values and the number of iterations of the neural network to fully ensure the correct training of the designed neural network. Fig. 10 shows the mean square error per number of iterations in which the outputs of the network and Talys were converged and the mean square error of 10 was obtained. The curves of Train, Validation, Test, and Best have been demonstrated by the best performance of epoch 57.

Fig. 11 shows the convergence of the neural network in terms of epochs to study the behavior of gradients, Mu, and validation-checks, such that their magnitudes in epoch 63 were 1.2709, 0.01, and 6, respectively. For gradient and Mu curves, the fluctuations were detected at the first and at the end of the epochs. However, the validation-check curve just revealed the variations at the end of epochs towards 63.

Fig. 12 shows the obtained error histogram. The correct error histogram should show a symmetrical situation around the point 0 (the yellow vertical line in the middle of the figure), as it can be seen that the error histogram of the network has been acceptably trained and has a relatively good symmetry around the zero point. It needs to be explained that the data are divided into 3 categories of training, validation and testing by the MATLAB software itself.

According to Fig. 13, it can be seen that the error regression is completely equal to 1, which indicates the complete correlation of the output data of the network and Talys. All categorizations of training, validation and testing show the estimated useful and effective mass of gallium-68.

4. Discussion

Fig. 14 compares the product energy-angle distributions for ^{68}Zn and ^{69}Ga targets in which differential data with respect to the angle and energy have been drawn as $d^2\sigma/d\Omega/dE$ (E_{out}) in terms of incident proton energy.

Fig. 15 shows the adaptation of Talys output and neural network output for the ^{68}Zn(p,n)^{68}Ga reaction contaminations.

Fig. 16 also shows the mean square error for the reaction contaminations in 3 categories of training, validation and testing at 263 epochs. While the epochs increased, the relevant error decreased as the best validation performance of these contaminations was found at epoch 257 by 0.00024376. In addition to that, Fig. 17 shows the training process of neural network for the reaction contaminations. The Gradient, Mu, and Validation behaviors for reaction contaminations demonstrated some fluctuations at beginning and end of the curves.

Fig. 18 compares the obtained error histogram for the reaction contaminations based on training, validation, and test situations around the zero point, where the plots are not symmetrical. In the following, Fig. 19 shows the regression of the error for the contaminations, that our output data for the contaminations caused by the reaction reached our desired result with a small percentage of error.

Here, the impact of each of the input parameters on the output material is identified. Based on neural network modeling, the effect of changing each of the input parameters, including time, radiation energy (ebeam), and the amount of reaction current (ibeam), on

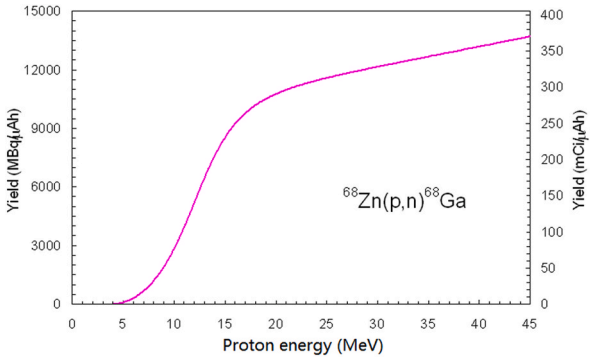

Fig. 6. Yield calculated from the recommended cross sections for the ^{68}Zn(p,n)^{68}Ga reaction.

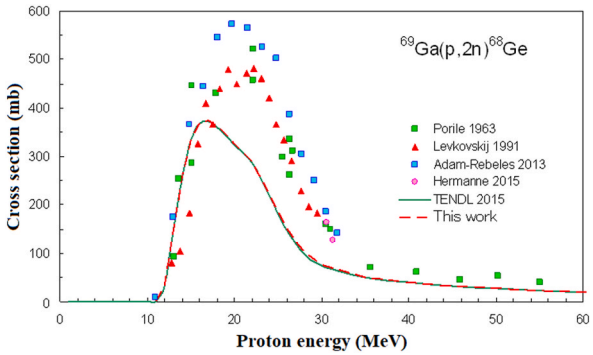

Fig. 7. The cross sections in terms of incident proton energy for the ^{69}Ga(p,2n)^{68}Ge reaction [26,38–40].

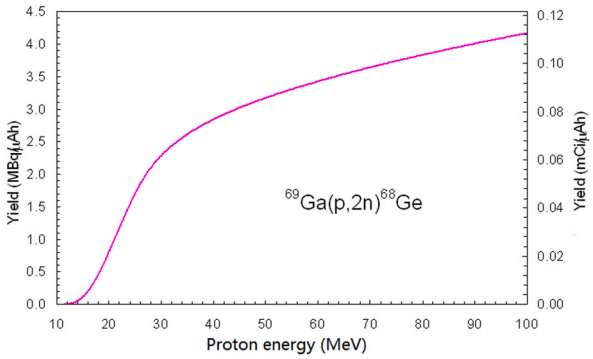

Fig. 8. Yield calculated from the recommended cross sections for the ^{69}Ga(p,2n)^{68}Ge reaction.

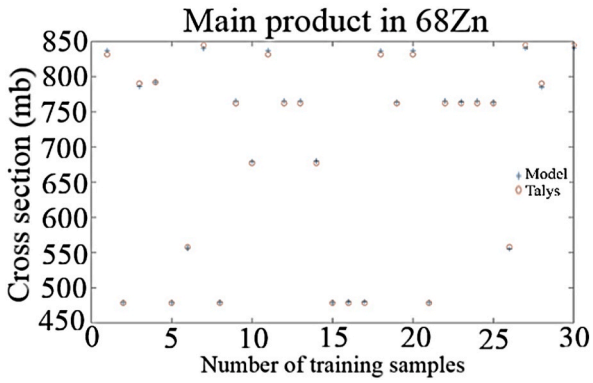

Fig. 9. Comparing the outputs from trained neural network model and Talys code for ^{68}Zn.

the output of useful material (main product) and the output of loss was investigated. The loss function is a tool that maps the amounts of some variables to a real number that intuitively signifies some "cost" related to those amounts. In backpropagation, the loss function computes the alteration between the network output and the expected output after a training instance is propagated across the network.

Fig. 20 shows the effect of the time parameter from 10 to 20 min on the useful output in the upper graph and on the pollutant output in the lower graph. It turned out that time is not an important parameter with regard to process optimization criteria. Simultaneously, Fig. 21 shows the amount of changes in ibeam on the output, which again had a steady-state graph and revealed that the change of this parameter had no particular effect on the output.

However, the most important graph is the effect of energy change on useful output and material pollution, shown in Fig. 22. In the upper part, which increases with energy up to 12 MeV, the useful material increased, but with further increases in energy, useful material decreased. Meanwhile, the lower part of Fig. 22 shows that with the increase in energy up to 12 MeV, the pollution has also increased, and from 12 MeV onwards, the trend of increasing extraneous substances has intensified rapidly. This shows that increasing

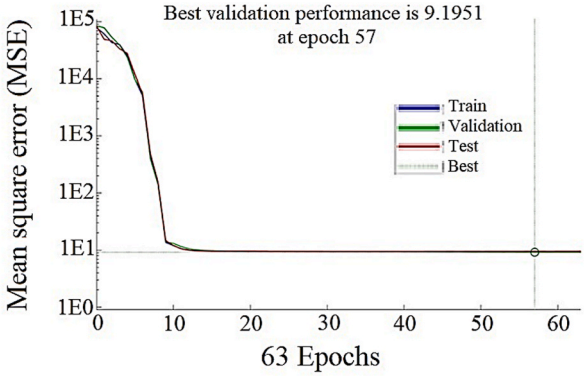

Fig. 10. Mean square error per iterations from network and Talys outputs for 63 epochs by best validation performance of epoch 57.

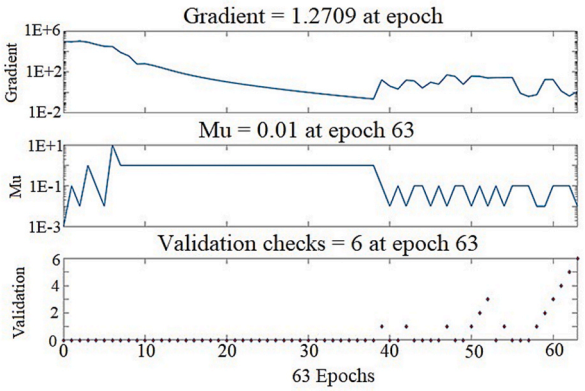

Fig. 11. The convergence of gradient, Mu, and validation curves for 63 epochs.

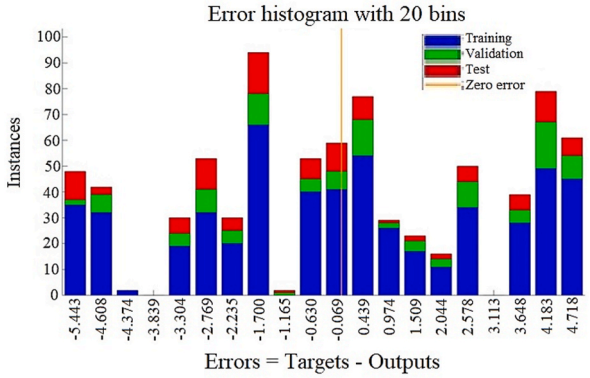

Fig. 12. The symmetric error histogram for training (blue), validation (green), and test (red) conditions around zero point of yellow vertical line.

energy from 12 MeV onwards has no effect on improving the process and somehow makes it worse.

One of the limitations of this design is that by changing the nuclear reaction conditions such as the type of target substance, its mass number, or sample dimensions, the trained model will not be able to predict the new process since no training data has been entered based on the nature of this process.

In view of the diverse possible uses of radiopharmaceuticals, radiochemical analysis is also of particular importance. Therefore, according to the specific radioisotope of this study, ^{68}Ga exists only in oxidation state III in aqueous solution and at physiological pH values. Given the recognized need to preclude the formation of insoluble $Ga(OH)_3$ and soluble $Ga(OH)^4$, the synthesis of ^{68}Ga-labeled radiopharmaceuticals is performed in the presence of weakly coordinating ligands like oxalate, acetate, and citrate, which limit the

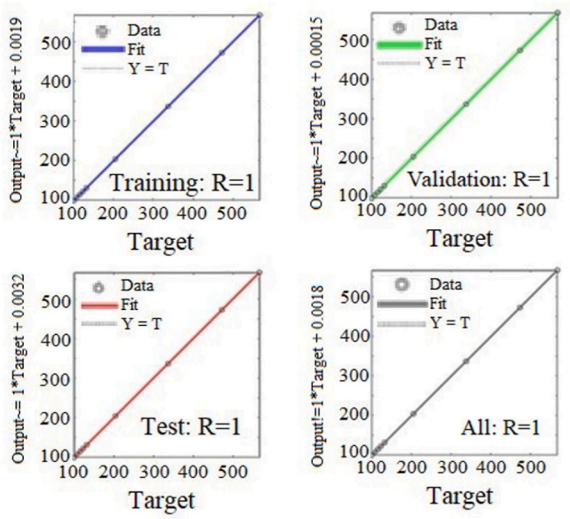

Fig. 13. Acquired error regression for training, validation and testing forms by positive correlation of 1.

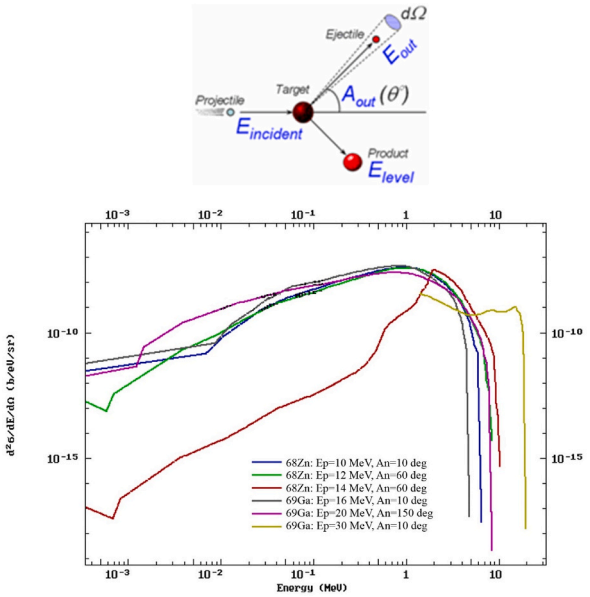

Fig. 14. The product energy-angle distributions for ^{68}Zn (incident proton energy of 10, 12, and 14 MeV) and ^{69}Ga (incident proton energy of 16, 20, and 30 MeV) targets.

kinetics of complex formation drastically reduce [41]. Gallium(III) is categorized into a hard Lewis acid and so binds to hard Lewis base donor atoms like oxygen and nitrogen, commonly forming six coordinate bonds in a nearly octahedral geometry. A number of hopeful ^{68}Ga tracers composed of large biomolecules, small molecules, and particles targeting biological activities like apoptosis, angiogenesis, and proliferation are presently in preclinical and experimental examination [42–44]. Regardless of whether clinics choose solid or liquid targets, a competent tool of purifying the ^{68}Ga from the irradiated ^{68}Zn is needed. The limitations of ^{68}Ga generated in the cyclotron are obvious: 1) a cyclotron with appropriate targets, 2) the simultaneous generation of ^{67}Ga and ^{66}Ga, and 3) the possibility of residual amounts of ^{68}Zn and other metal impurities influencing labeling effectiveness. These parameters place high demands on the target material, the proton current and energy, and the quality of the reagents as well as the ^{68}Zn/^{68}Ga separation techniques.

According to Karaj cyclotron in Iran - Cyclon30, IBA, Belgium – by maximum proton energy of 30 MeV, both reactions had an end-of-irradiation yield by 1437 and 5.13 MBq/μA.h for ^{68}Zn(p,n)^{68}Ga and ^{69}Ga(p,2n)^{68}Ge reactions, respectively.

Fig. 23 shows the evaluated cross-sections for ^{68}Zn(p,n)^{68}Ga reaction besides its impurities including ^{67}Ga and ^{65}Cu. As it is clear from Fig. 23, the impurity production of gallium-67 appears as a competing reaction up to 0.65 b around the energy of 20 MeV. For this reason, in this project, the amount of landing energy to investigate this reaction was considered between 10 and 14 MeV (blue curve in

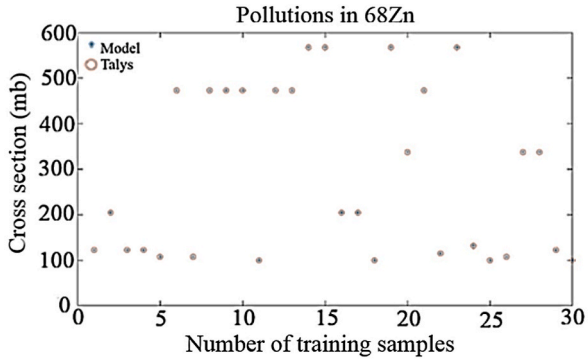

Fig. 15. Matching of Talys and network outputs for ^{68}Zn(p,n)^{68}Ga pollution.

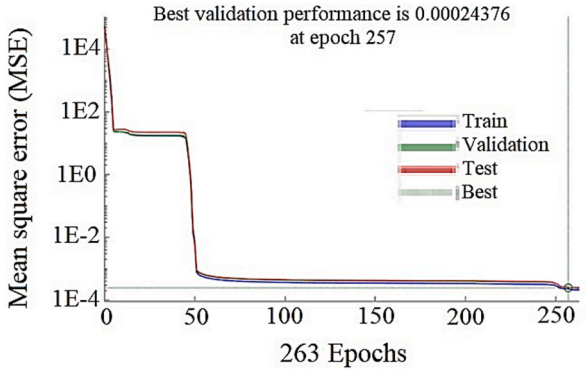

Fig. 16. Mean square error for reaction pollution in training, validation and testing forms.

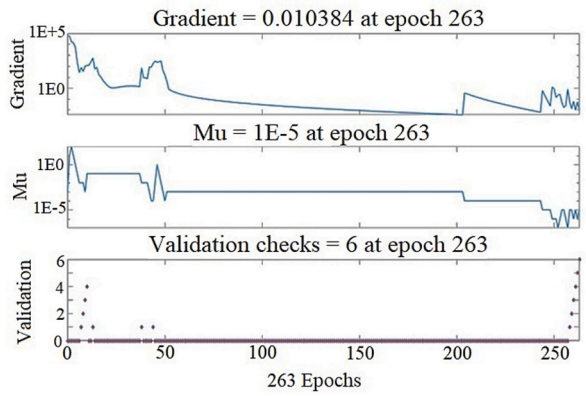

Fig. 17. The gradient, Mu, and validation curves for reaction pollution at 263 epochs.

bottom diagram) in order to reduce the generation impurities.

Fig. 24 shows the evaluated cross-sections for ^{69}Ga(p,2n)^{68}Ge→^{68}Ga reaction besides its impurities including ^{69}Ge and ^{66}Zn. As can be seen from Fig. 24, the impurity production of germanium-69 appears as a big and fierce competitor reaction up to 0.63 b between energy 5 and 15 MeV. But this reaction is more likely to occur at the energy range of 15–25 MeV (green curve in bottom diagram). Hence, the amount of incident proton energy to assess this reaction was considered between 15 and 30 MeV in order to diminish the induced impurities.

To fabricate ^{68}Ge/^{68}Ga generators and in order to separate ^{68}Ga from ^{68}Ge, two approaches are regularly employed. The first technique applies organic milieus from phenolic groups that create stable complexes with Ge(IV), preparing the elution of $^{68}Ga^{3+}$ as $^{68}GaCl_4^-$ with HCl as the eluent. On the other hand, an N-methylglucamine-established polymer and a 0.1 M tri-sodium citrate solution can be utilized as eluent [45]. The second technique applies inorganic oxide milieus like SnO_2, Al_2O_3, Sb_2O_5, TiO_2, and ZrO_2 and eluted

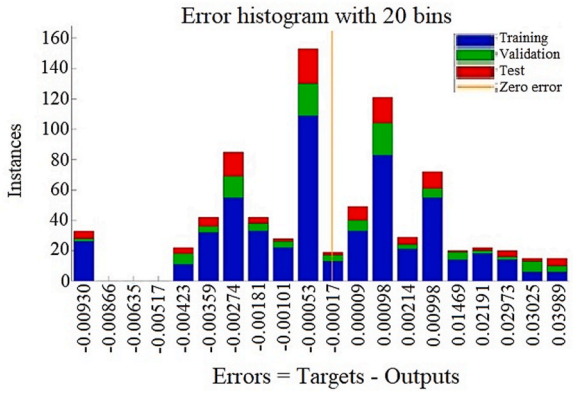

Fig. 18. The error histogram for derived pollution in Training (blue), Validation (green), and Test (red) conditions around zero point of yellow vertical line.

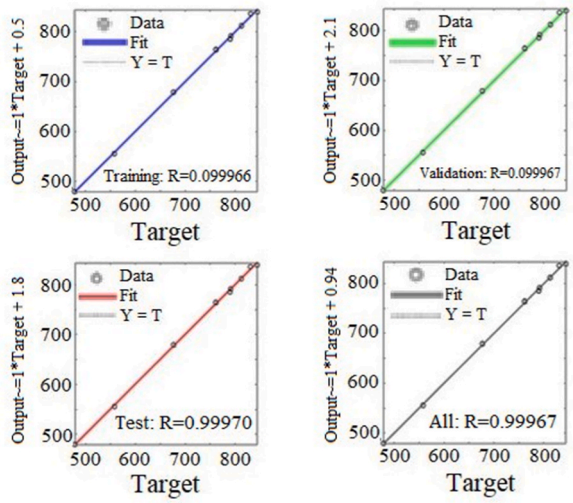

Fig. 19. The error regression of derived pollution in training, validation and testing forms.

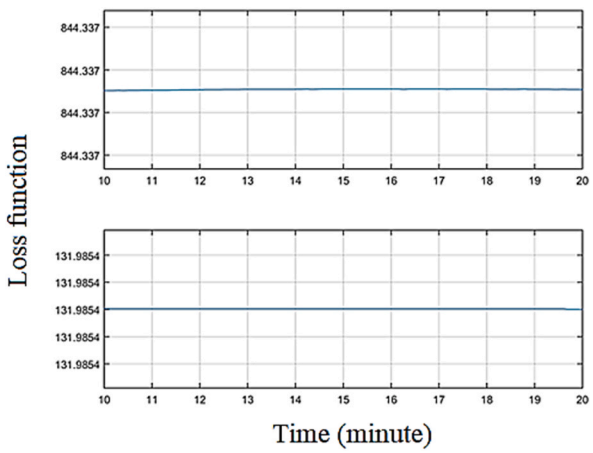

Fig. 20. Time impact on the process output for useful (Top) and pollution (bottom) materials.

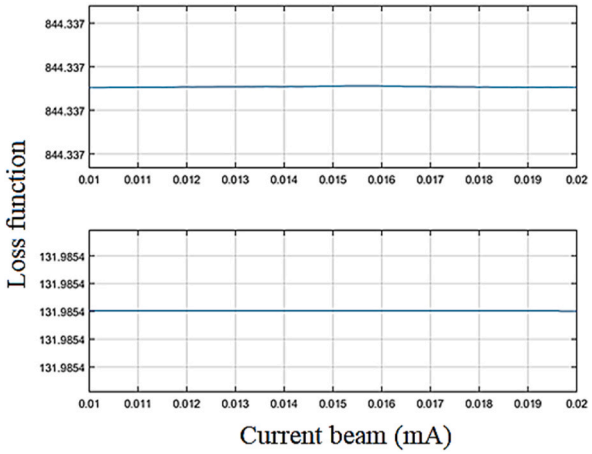

Fig. 21. I_{beam} impact on process output for useful (Top) and pollution (bottom) materials.

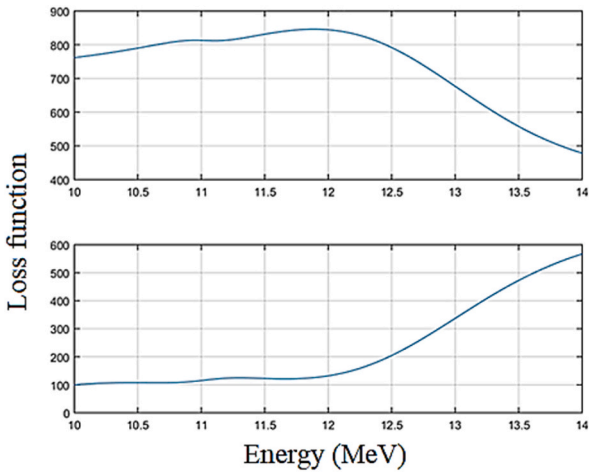

Fig. 22. Energy impact on process output for useful (Top) and pollution (bottom) materials.

with EDTA or HCl [46]. At present, the commercially existing "ionic" generators use HCl in dissimilar densities to elute ^{68}Ga in labeling reaction appropriately [47]. Regardless of which generator is utilized, the slow complexation, the large eluate volume, the kinetics, and the existence of metallic impurities like Fe^{3+}, Ti^{4+}, and Zn^{2+} that can complicate labeling perfusion with $^{68}Ga^{3+}$ must be taken into account as they compete for the similar chelators. Thus, post-processing cleaning approaches to remove contaminants have been detailed in recent researches [48–50].

For the routine generation of ^{68}Ge, two nuclear reactions are available: **1)** ^{66}Zn(α,2n)^{68}Ge in which the natural abundance of ^{66}Zn is 28 % and has been yielded up to 2 μCi/μA h by 35 MeV alpha energy per current beam and 1-h irradiation time; **2)** ^{69}Ga(p,2n)^{68}Ge in which ^{69}Ga has natural abundance about 60 % and has been yielded up to 20 μCi/μA h by 23 MeV proton energy [51]. Comparably, ^{69}Ga(p,2n)^{68}Ge has been here evaluated due to greater yields and chemical separation simplicity. By this approach, only two elements need to be separated from each other, while in (α,2n) reaction, a third element of zinc needs to be considered [52].

In our study, direct ^{68}Zn(p,n)^{68}Ga reaction and indirect ^{69}Ga(p,2n)^{68}Ge→^{68}Ga reaction were modeled to investigate the production yield and induced pollution via sub-models.

Mechanical, chemical, and thermal characteristics as well as corrosion and radiation resistance must be considered when choosing the target, because the target is exposed to high current irradiation and the power dissipated within the targets reaches amounts of about 200–1000 W or more. Target materials utilized for the generation of ^{68}Ge comprise Ga metal, GaAg, Ga_4Ni, and Ga_2O_3. The encapsulated Ga_2O_3 usage with high-current proton irradiation is ruled out because the oxide transitions from a hexagonal α-form to a monoclinic β-form at around 600 °C, accompanied by an increase in volume leading to capsule rupture. While the alloys usage as the target material, such as GaAg and Ga_4Ni, possesses the superiority in achieving good thermal conductivity, the need for a laborious chemical separation process to rid ^{68}Ge of concomitantly generated impurities discourages its usage. The outlook of utilizing Ga_2O_3 is hampered by the complications encountered in dissolving the irradiated target. Accordingly, the proposal of utilizing Ga metal seemed very attractive. Since Ga metal is so corrosive to Al, it is imperative that it be encapsulated, e.g. with Nb, because Ga would not react

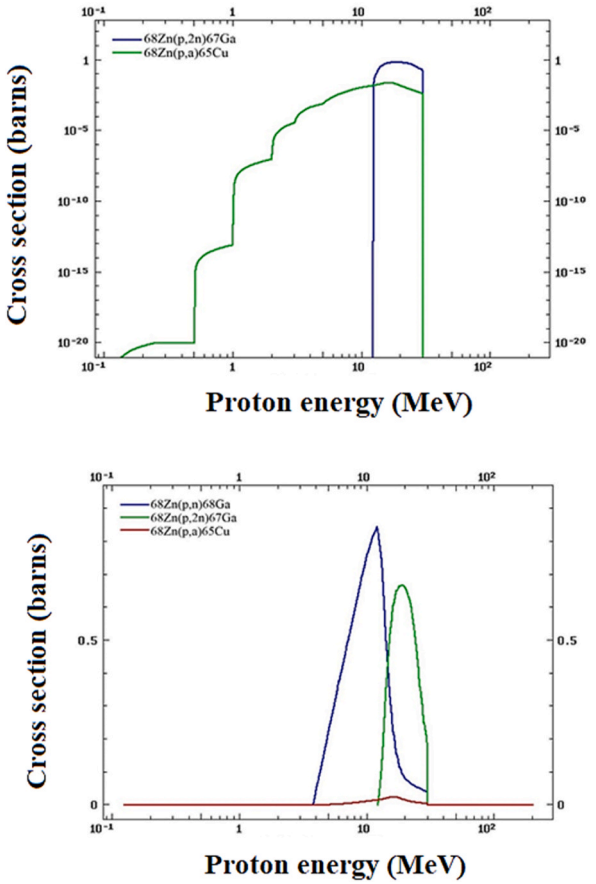

Fig. 23. Impurity reactions cross-sections for $^{68}Zn(p,n)^{68}Ga$: Top: only for competing reactions $^{68}Zn(p,\alpha)^{65}Cu$ and $^{68}Zn(p,2n)^{67}Ge$; Bottom: Comparing with main reaction.

with this kind of encapsulation.

Achieving satisfactory bevy yields requires proton energies greater than 20 MeV energy, high-current accelerators on the order of milli-Ampere, and long irradiation times of several days. Therefore, despite high demand, there are very few generator suppliers of ^{68}Ge. Four chief centers currently producing ^{68}Ge are: Cyclotron Co Ltd (Obninsk, Russia), iThemba Laboratories (South Africa), Los Alamos National Laboratory (USA), and Brookhaven National Laboratory (USA) [51]. These centers have been reported their generation capacities of approximately 18.5–74 GBq (0.5–2 Ci) of ^{68}Ge per bevy. Various separation methods have been executed to isolate micro-amounts of no-carried-added ^{68}Ge from macro-amounts of the irradiated target range from solvent extraction [53–55] and ion exchange chromatography to the use of organic [56] and inorganic [52,57] materials.

At BNL, production is done using ^{nat}Ga targets with about 45 MeV proton irradiations. For a distinctive bevy generation, 81 g of ^{nat}Ga metal encapsulated in a Nb container has been utilized and irradiation was done over a period of 4 weeks to attain 0.52 MBq/μA.h. The ^{68}Ge has been recovered from the target by extraction in 4 N HCl and 30 % H_2O_2 after cooling for two weeks. Additional purification is normally completed via solvent extraction with carbon tetrachloride and back extraction of ^{68}Ge in H_2O. It has been reported a total production yield around 85 % on a bevy yield of 33.3–51.8 GBq (900–1400 mCi) with radionuclide purity about 99.9 % and activity levels greater than 3.15 GBq/mL (85 mCi/ml) [58]. Situationally, 100 MeV proton beam have been utilized at Los Alamos National Laboratory (LANL) [59]. Ordinarily, a distinctive bevy generation requires about 4 g ^{nat}Ga metal encapsulated in a Nb container under period of 16–20 days' irradiation to reach 1.18 MBq/μA.h. The bevy yield at the end of irradiation (EOI) has been achieved about 55–70 GBq. Importantly, the chemical processing has been performed after 2 weeks of cooling by solvent extraction with CCl_4 and also re-extraction of ^{68}Ge in water, monitored through an ion-exchange purification stage with alumina [60]. A 66 MeV proton iraadiation has reported in the iThemba laboratories. For a distinct bevy generation, 5 g target with a generation ratio of 1.18 MBq (0.032 mCi) per μA.h has been experimentally utilized. The obtained radionuclide purity of the processed ^{68}Ge has been reported more than 99.9 % and the concluding product comprised less than 1 μg gallium per 37 MBq (1 mCi) of ^{68}Ge [61]. Meanwhile, a Ga–Ni alloy organized on Cu metal substructures has been designed as target material at Cyclotron Co. Ltd. in Obninsk, Russian Federation. The proton bombardments have been executed with a high intensity of several hundred micro-amperes of 23 MeV protons. The obtained ^{68}Ge with a high specific activity by more than 74 GBq (2 Ci) per mg of target besides 99.8 % radionuclide purity have been reported [62].

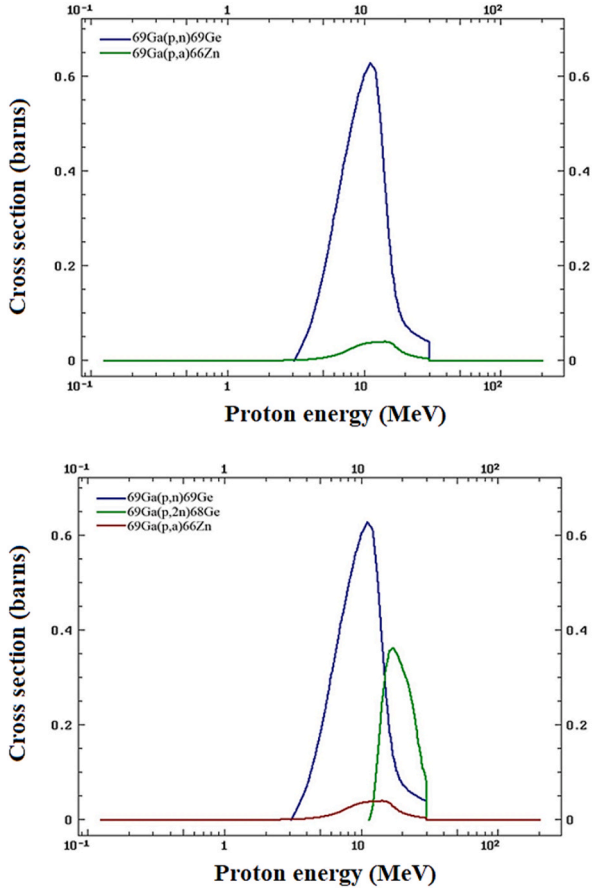

Fig. 24. Impurity reactions cross-sections for $^{69}Ga(p,2n)^{68}Ge \rightarrow ^{68}Ga$: Top: only for competing reactions $^{69}Ga(p,n)^{69}Ge$ and $^{69}Ga(p,\alpha)^{66}Zn$; Bottom: Comparing with main reaction.

The gallium ligands such as ^{68}Ga-DOTA-TOC and ^{68}Ga-DOTA-TATE are synthetic somatostatin analogs and bind with high affinity to the somatostatin receptor subtype 2, which is found in many cancers predominantly in meningioma, euroendocrine tumors, and neural crest tumors like ganglioneuroma, neuroblastoma, and pheochromocytoma. The substance can be crafted from a distinct dose kit using gallium collected from a $^{68}Ge/^{68}Ga$ generator. However, ^{68}Ga-DOTA-TOC was represented for somatostatin receptor PET imaging and attained greater detection ratios and improved spatial resolution than ^{111}In-pentetreotide scintigraphy [63].

Since radio-immunotherapy dosimetry besides nuclear imaging is a sophisticated attempt to compare the absorbed dose in tumors and normal tissues [64], up-to-date techniques are required to improve the therapeutic or diagnostic ratio [65–73]. Recently, bombarding $^{68}Zn(NO_3)_2$ as 1 M solution in dilute (0.2–0.3 M) HNO_3 has been executed by means of GE-PET-trace cyclotron and ^{68}Ga liquid targets [74]. The proton beam energy considered 14.3 MeV to diminish the pollutants or co-production of ^{67}Ga by $^{68}Zn(p,2n)^{67}Ga$ reaction without unduly affecting ^{68}Ga production yields. Besides, they appraised the properties of different beam currents 27–40 μA and beam times by 50–75 min, and finally measured crude production of ^{68}Ga. The $^{68}GaCl_3$ extraction was accomplished utilizing a 2-column solid-phase process on the GE-FAST-Lab-Developer platform. Consequently, they extracted $^{68}GaCl_3$ to label ^{68}Ga-PSMA-11 intended for clinical usage. Here in this research, a suitable alternative to diversify the ^{68}Ga supply is the direct generation of ^{68}Ga in a cyclotron-based method via the $^{68}Zn(p,n)^{68}Ga$ reaction. Decisively, there are two procedures to generate ^{68}Ga through this reaction on a cyclotron using solid target [75–77] and liquid target [78–80]. The liquid targets facilitate employment of ^{18}FDG-generation for different applications and centers as they have an identical workflow to fluoride (^{18}F) generation and are compatible with laboratory setups in current PET radiopharmaceutical manufacturing sites. Nonetheless, solid targets normally impose incremental demands on substructure and local center expertise, and also it brings about greater level of ^{68}Ga production yield, for instance, several GBq/Ci [76, 81]. Regardless of whether they choose solid or liquid targets, an effective tool for ^{68}Ga purifying from the bombarded ^{68}Zn is required. The limitations of ^{68}Ga generated in the cyclotron are noticeable: 1) a compact cyclotron with proper targets, 2) the simultaneous production of ^{66}Ga and ^{67}Ga as contaminants, and 3) the possibility of residual amounts of ^{68}Zn besides additional metal impurities that influence the labeling productivity. These issues create extraordinary requests for the proton beam current and energy, the designed target material, the quality of the reagents, and lastly for the $^{68}Zn/^{68}Ga$ separation ways.

Recently, Naik et al. [24] measured the cross sections for $^{68}Zn(p,n)^{68}Ga$ reaction for various proton energies from 8.6 MeV to 17.7 MeV with an overall uncertainty of 7.7 %–9.6 %. Their reported cross sections were 948 mb and 390 mb for incident proton energies of

12.1 MeV and 15.1 MeV, respectively. At these proton energies, the theoretical values from Talys are 844 mb and 296 mb correspondingly. In our study, the relevant cross sections of this reaction were 755 mb and 561 mb, respectively, for incident proton energies of 10 MeV and 14 MeV with an overall uncertainty of 7.4 %. Among the limitations of the presented work, we can highlight the nature of physics card in the collision of protons with the target, the number of incident particles and the problem of irradiation time. Also, the history of tracking particles with different absorption interactions and elastic and inelastic scattering can be examined in a more detailed estimate. On the other hand, when estimating pollution and competing reactions, using a larger number of sublayers or even different neural network training methods can be analyzed to reduce the error.

The main goal of this research was to use the outputs of Talys code to simulate the nuclear bombardment and reaction process using the neural network model. Therefore, a comprehensive database was created by running the Talys code under different conditions based on the type of Zn material, totaling six thousand different runs. Finally, the Talys code outputs were automatically read by the MATLAB software and the necessary information was extracted. Two feed-forward neural networks were trained with the "back-propagation-error" model in a form that can model the chief output of the process and the equivalent outputs of pollution or process loss based on the input parameters and their changes. The only assumption made was to create inputs within the practically acceptable range given the model, so that the software was able to train this process with reasonable precision through the neural network. It must be explained that using a neural network instead of Talys code, in addition to easy modeling, also provides the possibility of high-speed process optimization by appropriate software.

5. Conclusion

By virtue of short half-life of most radioisotopes derived from generators, the use of distinct kit formulation approaches looks like wise as they would diminish reagent procurement, human error, and setup time, as well as it simplifies cleanup and operation and also eliminates the possibility of pollution. Another benefit of kits is the facilitation of reagent management. Rather than handling various reagents separately, the radiopharmaceutical only requires to accomplish the kit as a distinct entity, significantly facilitating FDA regulations approval for manufacturing PET tracers and human injection. Kit design policies are increasingly giving the clinicians and scientists who require them the ability to make PET tracers. Utilizing $^{68}Ge/^{68}Ga$ generators has great demands in PET centers for the following reasons:

1) The 270-day half-life of ^{68}Ge guarantees the possibility of using the generator for extended periods of time, possibly up to 1 year or more.
2) The decay properties of the short-lived daughter ^{68}Ga ($t½ = 68$ min, 11 % EC, 89 % $\beta+$, $E_{\beta+,\,max} = 1.97$ MeV) are suitable for PET clinics.

In addition to the radiochemical properties, from a physical point of view, the precise estimation of the proton interaction cross-section with the zinc-68 and gallium-69 targets and then the estimation of the production yield is of utmost importance. In this study, the computed yields for $^{68}Zn(p,n)^{68}Ga$ reaction were 2820 and 7600 MBq/μA.h for 10 and 14 MeV proton energy, respectively. Meanwhile, the computed yields for $^{69}Ga(p,2n)^{68}Ge$ reaction were 0.116 and 2.29 MBq/μA.h for 15 and 30 MeV proton energy, respectively. According to Karaj cyclotron in Iran, by maximum proton energy of 30 MeV, both reactions had an end-of-irradiation yield by 1437 and 5.13 MBq/μA.h, correspondingly. The (p,2n) reaction generated higher saturation activity of positron emitters than (p,n) reaction.

Since the ^{68}Ga has a physical half-life of 68 min and possesses a rapid blood clearance, rapid diffusion, and a proper localization to the target, therefore, it counterparts the biological half-life of various peptides utilized for imaging. The ability of $^{68}Ga^{3+}$ to produce stable complex with different ligands that comprise nitrogen and oxygen as donor atoms represents the prospect of complexation with a various chelating agents besides several macromolecules with substantial clinical capability. This study attempted to estimate the order of errors in the competing reactions and impurities of the main product by training the neural network, so that a method can be chosen to better estimate the main product or even increase it by fundamentally revising the phases of radiopharmaceutical production.

Ethical approval

Not required.

Data availability statement

No data was used for the research described in the article. All data required to support the results and conclusions of the study have been provided here with the submission.

CRediT authorship contribution statement

Abdollah Khorshidi: Writing – review & editing, Writing – original draft, Visualization, Validation, Supervision, Software, Resources, Project administration, Methodology, Investigation, Funding acquisition, Formal analysis, Data curation, Conceptualization.

Declaration of competing interest

The authors declare that they have no known competing financial interests or personal relationships that could have appeared to influence the work reported in this paper.

Acknowledgements

Due to the tireless efforts of Qasem Soleimani, this research has been donated to the Soleimani Maktab.

Appendix A. Supplementary data

Supplementary data to this article can be found online at https://doi.org/10.1016/j.heliyon.2024.e31499.

References

[1] A. Khorshidi, Exploration of adiabatic resonance crossing through neutron activator design for thermal and epithermal neutron formation in99Mo production and BNCT applications, Cancer Biother. Rad. 30 (8) (2015) 317–329, https://doi.org/10.1089/cbr.2014.1734.
[2] A. Khorshidi, Gold nanoparticles production using reactor and cyclotron based methods in assessment of 196,198 Au production yields by 197 Au neutron absorption for therapeutic purposes, Mater. Sci. Eng. C 68 (2016) 449–454, https://doi.org/10.1016/j.msec.2016.06.018.
[3] A. Khorshidi, Accelerator driven neutron source design via beryllium target and 208Pb moderator for boron neutron capture therapy in alternative treatment strategy by Monte Carlo method, J. Cancer Res. Therapeut. 13 (3) (2017) 456–465, https://doi.org/10.4103/0973-1482.179180.
[4] A. Khorshidi, Neutron activator design for 99Mo production yield estimation via lead and water moderators in transmutation's analysis, Instrum. Exp. Tech. 61 (2018) 198–204, https://doi.org/10.1134/S002044121802015X.
[5] A. Khorshidi, B. Khosrowpour, S.H. Hosseini, Determination of defect depth in industrial radiography imaging using MCNP code and SuperMC software, Nucl. Eng. Technol. 52 (7) (2020) 1597–1601, https://doi.org/10.1016/j.net.2019.12.010.
[6] A. Khorshidi, Assessment of SPECT images using UHRFB and other low-energy collimators in brain study by Hoffman phantom and manufactured defects, The European Physical Journal Plus 135 (2020) 261, https://doi.org/10.1140/epjp/s13360-020-00238-6.
[7] A. Khorshidi, M. Ashoor, New deformity outline on the breast radiation therapy for diminishing absorbed dose ratio, Brazilian Journal of Radiation Sciences 11 (3) (2023) 1–12, https://doi.org/10.15392/2319-0612.2023.2281.
[8] A. Khorshidi, A. Rajaee, M. Ahmadinejad, M. Ghoranneviss, M. Ettelaee, Low energy electron generator design and depth dose prediction for micro-superficies tumors treatment purposes, Phys. Scripta 89 (2014) 095001, https://doi.org/10.1088/0031-8949/89/9/095001.
[9] Historical Timeline, Important Moments in the History of Nuclear Medicine. Society of Nuclear Medicine and Molecular Imaging. https://www.snmmi.org/AboutSNMMI/Content.aspx?ItemNumber=4175.
[10] A. Tantillo, Celebrating 50 Years of evaluated nuclear data. https://www.bnl.gov/newsroom/news.php?a=212873, 2018.
[11] G.I. Gleason, A positron cow, Int. J. Appl. Radiat. Isot. 8 (2–3) (1960) 90–94, https://doi.org/10.1016/0020-708X(60)90052-1.
[12] A. Khorshidi, Radiochemical parameters of molybdenum-99 transmutation in cyclotron-based production method using a neutron activator design for nuclear-medicine aims, The European Physical Journal Plus 134 (2019) 249, https://doi.org/10.1140/epjp/i2019-12568-3.
[13] A. Khorshidi, Accelerator-based methods in radio-material 99Mo/99mTc production alternatives by Monte Carlo method: the scientific-expedient considerations in nuclear medicine, J. Multiscale Model. (JMM) 11 (1) (2020) 1930001, https://doi.org/10.1142/S1756973719300016.
[14] A. Khorshidi, Nano Yttrium-90 and Rhenium-188 production through medium medical cyclotron and research reactor for therapeutic usages: a Simulation study, Nucl. Eng. Technol. 55 (5) (2023) 1871–1877, https://doi.org/10.1016/j.net.2023.02.013.
[15] A. Koning, S. Hilaire, S. Goriely, TALYS-1.96/2.0, Simulation of Nuclear Reactions, IAEA, 2021. https://www-nds.iaea.org/talys/tutorials/talys_v1.96.pdf. https://www-nds.iaea.org/talys/.
[16] F. Roesch, P.J. Riss, The renaissance of the 68 Ge/68 Ga radionuclide generator initiates new developments in 68 Ga radiopharmaceutical chemistry, Curr. Top. Med. Chem. 10 (16) (2010) 1633–1668, https://doi.org/10.2174/156802610793176738.
[17] Davey PRWJ, Paterson BM. Modern Developments in Bifunctional Chelator Design for Gallium Radiopharmaceuticals. Molecules 202; 28 (1): 203. https://doi.org/10.3390/molecules28010203.
[18] G. Crișan, N.S. Moldovean-Cioroianu, D.G. Timaru, G. Andrieș, C. Căinap, V. Chiș, Radiopharmaceuticals for PET and spect imaging: a literature review over the last decade, Int. J. Mol. Sci. 23 (2022) 5023, https://doi.org/10.3390/ijms23095023.
[19] P. Gavriilidis, M. Koole, S. Annunziata, F.M. Mottaghy, R. Wierts, Positron range corrections and denoising techniques for gallium-68 PET imaging: a literature review, Diagnostics 12 (10) (2022) 2335, https://doi.org/10.3390/diagnostics12102335.
[20] A. Sanchez-Crespo, Comparison of Gallium-68 and Fluorine-18 imaging characteristics in positron emission tomography, Appl. Radiat. Isot. 76 (2013) 55–62, https://doi.org/10.1016/j.apradiso.2012.06.034.
[21] Neural Network Architectures, 2023. https://www.mathworks.com/help/deeplearning/ug/neural-network-architectures.html.
[22] Create and train a feedforward neural network. https://www.mathworks.com/help/thingspeak/create-and-train-a-feedforward-neural-network.html, 2023.
[23] Multilayer shallow neural networks and backpropagation training. https://www.mathworks.com/help/deeplearning/ug/multilayer-neural-networks-and-backpropagation-training.html?searchHighlight=Back-Propagation%20&s_tid=srchtitle_support_results_1_Back-Propagation%20, 2023.
[24] H. Naik, S.V. Suryanarayana, M.S. Murali, R.K. Noy, Excitation function of 68Zn(p, n)68Ga reaction for the production of 68Ga, J. Radioanal. Nucl. Chem. 324 (2020) 285–289, https://doi.org/10.1007/s10967-020-07037-4.
[25] G.V. Kotelnikova, G.N. Lovchikova, O.A. Salʹnikov, S.P. Simakov, A.M. Trufanov, N.I. Fetisov, The investigation of neutron energy spectra for 68Zn(p, n) 68Ga reaction, Fiz.-Energ. Institut. Obninsk report 1141 (1980) 1.
[26] V.N. Levkovskij, Middle Mass Nuclides (A= 40–100) Activation Cross-Sections by Medium Energy (E= 10–50 MeV) Protons and Alpha Particles (Experiment and Systematics), Inter-vesi, Moscow, Russia, 1991.
[27] A.E. Antropov, V.P. Gusev, Y. Zhuravlev, P.P. Zarubin, A.A. Kolozhvari, A.V. Smirnov, Total cross sections of (p,n) reaction on the nuclei of isotopes nickel and zink at E (p) ¼5–6, MeV. Bull. Russ. Acad. Sci.: Phys. 56 (1992) 1829.
[28] Y.Y. Zhuravlev, P.P. Zarubin, Y.V. Zejts, A.A. Kolozhvari, I.V. Shelgunov, Excitation functions of the (p, n) reaction on nuclei of isotopes Zn at E p= 5.7-6.8 MeV, Izv. Akad. Nauk, Ser. Fiz. 59 (1) (1995) 118–121.
[29] V.M. Vinogradov, Y.Y. Zhuravlev, P.P. Zarubin, Excitation functions of the (pn) reaction on zinc isotopes in E p= 4.9-5.9 MeV energy range, Izvestiya Akademii Nauk-Rossijskaya Akademiya Nauk. Seriya Fizicheskaya 57 (5) (1993) 154–159.
[30] J.P. Blaser, F. Boehm, P. Marmier, D.C. Peaslee, Fonctions d'excitation de la reaction (p, n), Helv. Phys. Acta 24 (1951) 3–38.
[31] M. Hille, P. Hille, M. Uhl, W. Weisz, Excitation functions of (p, n) and (α, n) reactions on Ni, Cu and Zn, Nucl. Phys. 198 (2) (1972) 625–640.
[32] Howe HA, (p, n) cross sections of copper and zinc, Phys. Rev. 109 (6) (1958) 2083–2085.

[33] M.T. Esat, R.H. Spear, J.L. Zyskind, M.H. Shapiro, W.A. Fowler, J.M. Davidson, Test of global Hauser-Feshbach calculations for proton-induced reactions on Zn 68, Phys. Rev. C 23 (4) (1981) 1822–1825.
[34] F. Tárkányi, F. Szelecsényi, Z. Kovács, S. Sudár, Excitation functions of proton induced nuclear reactions on enriched 66Zn, 67Zn and 68Zn: production of 67Ga and 66Ga, Radiochim. Acta 50 (1–2) (1990) 19–26.
[35] F. Szelecsényi, Z. Kovács, K. Nagatsu, K. Fukumura, K. Suzuki, K. Mukai, Investigation of direct production of 68Ga with low energy multiparticle accelerator, Radiochim. Acta 100 (1) (2012) 5–11.
[36] C.H. Johnson, C.C. Trail, A. Galonsky, ThresholDs for (p, n) reactions on 26 intermediate-weight nuclei, Phys. Rev. vol. 136 (6B) (1964) B1719–B1729.
[37] F.S. Al-Saleh, K.S. Al Mugren, A. Azzam, Excitation function measurements and integral yields estimation for natZn (p x) reactions at low energies, Appl. Radiat. Isot. 65 (10) (2007) 1101–1107.
[38] N.T. Porile, S. Tanaka, H. Amano, M. Furukawa, S. Iwata, M. Yagi, Nuclear reactions of Ga69 and Ga71 with 13–56 MeV protons, Nucl. Phys. 43 (1963) 500–522.
[39] R. Adam-Rebeles, A. Hermanne, P. Van den Winkel, L. De Vis, R. Waegeneer, F. Tárkányi, S. Takacs, M.P. Takács, 68Ge/68Ga production revisited: excitation curves, target preparation and chemical separation–purification, Radiochimca Acta 101 (8) (2013) 481–489.
[40] A. Hermanne, R. Adam-Rebeles, F. Tárkányi, S. Takacs, F. Ditroi, Proton and deuteron induced reactions on natGa: experimental and calculated excitation functions, Nucl. Instrum. Methods Phys. Res. Sect. B Beam Interact. Mater. Atoms 359 (2015) 145–154.
[41] M.D. Bartholomä, Recent developments in the design of bifunctional chelators for metal-based radiopharmaceuticals used in Positron Emission Tomography, Inorg. Chim. Acta. 389 (2012) 36–51.
[42] I. Velikyan, O. Lindhe, Preparation and evaluation of a 68Ga-labeled RGD-containing octapeptide for noninvasive imaging of angiogenesis: biodistribution in non-human primate, Am J Nucl Med Mol Imaging 8 (2018) 15–31.
[43] S.A. Esfahani, S. Salcedo, P. Heidari, O.A. Catalano, R. Pauplis, J. Hesterman, J.F. Kronauge, U. Mahmood, A phase one, single-dose, open-label, clinical safety and PET/MR imaging study of 68Ga-DOTATOC in healthy volunteers, Am J Nucl Med Mol Imaging 7 (2017) 53–62.
[44] A. Mojtahedi, A. Alavi, S. Thamake, R. Amerinia, D. Ranganathan, I. Tworowska, E.S. Delpassand, Assessment of vulnerable atherosclerotic and fibrotic plaques in coronary arteries using 68Ga-DOTATATE PET/CT, Am J Nucl Med Mol Imaging 5 (2015) 65–71.
[45] M. Nakayama, M. Haratake, M. Ono, T. Koiso, K. Harada, H. Nakayama, S. Yahara, Y. Ohmomo, Y. Arano, A new 68Ge/68Ga generator system using an organic polymer containing N-methylglucamine groups as adsorbent for 68Ge, Appl. Radiat. Isot. 58 (1) (2003) 9–14.
[46] R. Lambrecht, M. Sajjad, Accelerator derived radionuclive generators, Radiochim. Acta 43 (1978) 171–179.
[47] A. Amor-Coarasa, M. Schoendorf, M. Meckel, S. Vallabhajosula, J.W. Babich, Comprehensive quality control of the ITG 68Ge/68Ga generator and synthesis of 68Ga-dotatoc and 68Ga-PSMA-HBED-CC for clinical imaging, J. Nucl. Med. 57 (9) (2016) 1402–1405.
[48] C. Decristoforo, R. Knopp, E. von Guggenberg, M. Rupprich, T. Dreger, A. Hess, I. Virgolini, R. Haubner, A fully automated synthesis for the preparation of 68Ga-labelled peptides, Nucl. Med. Commun. 28 (11) (2007) 870–875.
[49] K.P. Zhernosekov, D.V. Filosofov, R.P. Baum, P. Aschoff, H. Bihl, A.A. Razbash, M. Jahn, M. Jennewein, F. Rosch, Processing of generator-produced 68Ga for medical application, J. Nucl. Med. 48 (10) (2007) 1741–1748.
[50] N.S. Loktionova, A.N. Belozub, D.V. Filosofov, K.P. Zhernosekov, T. Wagner, A. Turler, F. Rosch, Improved column-based radiochemical processing of the generator produced 68Ga, Appl. Radiat. Isot. 69 (7) (2011) 942–946.
[51] Production of long lived parent radionuclides for generators: 68Ge, 82Sr, 90Sr, and 188W, International Atomic Energy Agency (IAEA) publication 10-00628, Vienna, Austria, 2010.
[52] P.J. Pao, D.J. Silvester, S.L. Waters, A new method for the preparation of 68Ga-generators following proton bombardment of gallium oxide targets, J. Radioanal. Nucl. Chem. 64 (1981) 267–272.
[53] M. Fassbender, F.M. Nortier, D.R. Phillips, V.T. Hamilton, C. Heaton, D.J. Jamriska, J.J. Kitten, L.R. Pitt, L.L. Salazar, F.O. Valdez, E.J. Peterson, Some nuclear chemical aspects of medical generator nuclide production at the Los Alamos hot cell facility, Radiochim. Acta 92 (2004) 237–243.
[54] Loc'h C, B. Maziere, D. Comar, R. Knipper, A new preparation of germanium 68, Int. J. Appl. Radiat. Isot. 33 (1982) 267–270.
[55] T.N. van der Walt, C. Vermeulen, Thick targets for the production of some radionuclides and the chemical processing of these targets at iThemba LABS, Nucl. Instrum. Methods Phys. Res. 521 (2004) 171–175.
[56] C. Naidoo, T.N. van der Walt, H.G. Raubenheimer, Cyclotron production of 68Ge with a Ga2O target, J. Radioanal. Nucl. Chem. 253 (2002) 221–225.
[57] W.L. Cheng, Y. Jao, C.S. Lee, A.R. Lo, Preparation of 68Ge/68Ga generator with a binary Ga/Ag electrodepositions as solid target, J. Radioanal. Nucl. Chem. 245 (2000) 25–30.
[58] G.E. Meinken, S. Kurczak, L.F. Mausner, K.L. Kolsky, S.C. Srivastava, Production of high specific activity 68Ge at brookhaven national laboratory, J. Radioanal. Nucl. Chem. 263 (2005) 553–557.
[59] EJ Peterson, Accelerator radioisotopes save lives: the isotope production facility at Los Alamos, Los Alamos Science 30 (30) (2006) 112–123. Available at: https://library.lanl.gov/cgi-bin/getfile?30-14.pdf.
[60] D.R. Philips, Radioisotope Production at Los Alamos National Laboratory, Presented at Specialization School on Health Physics, Milan, 2002. Available at: www.mi.infn.it/conferences/phillips/Lanl.pdf.
[61] The National Isotope Development Center (NIDC) Product Catalog, Available at: https://www.isotopes.gov/products/germanium.
[62] B.G. Bulduk, V. Yasakçı, E. Tutun, P. Ünak, Ö. Aras, INVESTIGATIONS OF 44Ti PRODUCTION FOR 44Ti/44Sc RADIONUCLIDE GENERATOR, Turkish Journal of Nuclear Sciences 34 (1) (2022) 30–39.
[63] R.A. Feelders, L.J. Hofland, D.J. Kwekkeboom, S.W. Lamberts, W.W. de Herder, in: G. Fink, D.W. Pfaff, J.E. Levine (Eds.), Handbook of Neuroendocrinology, Chapter 35 - Neuroendocrine Tumors, Academic Press, 2012, pp. 761–778, https://doi.org/10.1016/B978-0-12-375097-6.10035-6.
[64] S.E. Strand, M. Ljungberg, J. Tennvall, K. Norrgren, M. Garkavij, Radio-immunotherapy dosimetry with special emphasis on SPECT quantification and extracorporeal immuno-adsorption, Med. Biol. Eng. Comput. 32 (1994) 551–561, https://doi.org/10.1007/BF02515314.
[65] Tabrizi S. Hariri, M. Ramezani, S.A.H. Feghhi, P. Geramifar, In vitro evaluation of an iodine radionuclide dosimeter (IRD) for continuous patient monitoring, Med. Biol. Eng. Comput. 58 (2020) 763–769, https://doi.org/10.1007/s11517-020-02129-5.
[66] M. Kusy, B. Obrzut, J. Kluska, Application of gene expression programming and neural networks to predict adverse events of radical hysterectomy in cervical cancer patients, Med. Biol. Eng. Comput. 51 (2013) 1357–1365, https://doi.org/10.1007/s11517-013-1108-8.
[67] K. Balasundaram, S. Masse, K. Nair, K. Umapathy, A classification scheme for ventricular arrhythmias using wavelets analysis, Med. Biol. Eng. Comput. 51 (2013) 153–164, https://doi.org/10.1007/s11517-012-0980-y.
[68] A. Khorshidi, Tumor segmentation via enhanced area growth algorithm for lung CT images, BMC Med Imaging 23 (2023) 189, https://doi.org/10.1186/s12880-023-01126-y.
[69] J. Das, Barman, S. Mandal, Classification of Homo sapiens gene behavior using linear discriminant analysis fused with minimum entropy mapping, Med. Biol. Eng. Comput. 59 (2021) 673–691, https://doi.org/10.1007/s11517-021-02324-y.
[70] M. Ashoor, A. Khorshidi, Modeling modulation transfer function based on analytical functions in imaging systems, Eur. Phys. J. Plus 138 (2023) 249, https://doi.org/10.1140/epjp/s13360-023-03884-8.
[71] M. Ashoor, A. Khorshidi, Modelling cardiovascular system using Fermi functions on capillary bed, Sadhana 48 (2023) 151, https://doi.org/10.1007/s12046-023-02229-6.
[72] A. Khorshidi, Segmentation of tumor region in respiratory disease by extended algorithm, Int. J. Mod. Phys. C 34 (12) (2023) 1–20, https://doi.org/10.1142/S0129183123501644.
[73] G.J. Ramírez-Nava, C.L. Santos-Cuevas, I. Chairez, L. Aranda-Lara, Multimodal molecular 3D imaging for the tumoral volumetric distribution assessment of folate-based biosensors, Med. Biol. Eng. Comput. 56 (2018) 1135–1148, https://doi.org/10.1007/s11517-017-1755-2.
[74] M.E. Rodnick, C. Sollert, D. Stark, et al., Cyclotron-based production of 68Ga, [68Ga]GaCl3, and [68Ga]Ga-PSMA-11 from a liquid target, EJNMMI radiopharm. chem. 5 (2020) 25, https://doi.org/10.1186/s41181-020-00106-9.

[75] A. Boschi, P. Martini, V. Costa, A. Pagnoni, L. Uccelli, C. Santini, et al., Interdisciplinary tasks in the cyclotron production of Radiometals for medical applications. The case of 47Sc as example, Molecules 24 (2019) 1–14.
[76] C. Schweinsberg, A. Johayem, A. Llamazares, K. Gagnon, The first curie-quantity production of [68Ga]Ga-PSMA-HBED-CC, J. Label. Compd. Radiopharm. 62 (S1) (2019) P121.
[77] S. Zeisler, A. Limoges, J. Kumlin, J. Siikanen, C. Hoehr, Fused zinc target for the production of gallium radioisotopes, Instruments 3 (2019) 10.
[78] S.J.C. do Carmo, P.J.H. Scott, F. Alves, Production of radiometals in liquid targets, EJNMMI Radiopharm Chem. 5 (2020) 2.
[79] M.K. Pandey, J.F. Byrne, H. Jiang, A.B. Packard, T.R. DeGrado, Cyclotron production of 68Ga via the 68Zn(p, n)68Ga reaction in aqueous solution, Am J Nucl Med Mol Imaging 4 (2014) 303–310.
[80] E. Oehlke, C. Hoehr, X. Hou, V. Hanemaayer, S. Zeisler, M.J. Adam, et al., Production of Y-86 and other radiometals for research purposes using a solution target system, Nucl. Med. Biol. 42 (2015) 842–849.
[81] M. Lin, G.J. Waligorski, C.G. Lepera, Production of curie quantities of 68Ga with a medical cyclotron via the 68Zn(p, n)68Ga reaction, Appl. Radiat. Isot. 133 (2018) 1–3.